NDT&E International 141 (2024) 102992

Contents lists available at ScienceDirect

NDT and E International

journal homepage: www.elsevier.com/locate/ndteint

Evaluation of nonlinear interface areas in a multiple scattering medium by Nonlinear Coda Wave Interferometry (NCWI): Experimental studies

Guangzhi Chen [a,b,c,*], Odile Abraham [b], Damien Pageot [b], Olivier Durand [b], Mathieu Chekroun [c], Vincent Tournat [c]

[a] School of Electronic and Information Engineering, Changshu Institute of Technology, Changshu 215500, China
[b] GERS-GeoEND, Université Gustave Eiffel, IFSTTAR, CS5004, F-44344 Bouguenais, France
[c] Laboratoire d'Acoustique de l'Université du Mans (LAUM), UMR 6613, Institut d'Acoustique - Graduate School (IA-GS), CNRS, Le Mans Université, France

ARTICLE INFO

Keywords:
Nonlinear Coda Wave Interferometry (NCWI)
Contact Acoustic Nonlinearity (CAN)
Experimental setup
Non-Destructive Testing (NDT)
Nonlinear acoustics

ABSTRACT

This paper aims to investigate the application of the Nonlinear Coda Wave Interferometry (NCWI) method in evaluating the nonlinear interface areas in highly heterogeneous materials. An experimental protocol is proposed for quantitatively analyzing the nonlinear interface effects in a multiple scattering medium. The experimental design involves a perforated aluminum plate with a surface ratio of circular voids equal to 17.63%, some of which are threaded to accommodate screws. The nonlinear contacts between the screws and the perforated plate are highlighted by a strong pump wave and investigated using the coda waves. Drawing upon prior numerical simulation findings (Chen et al., 2021), it is anticipated that the CWI observables (namely, the relative variation of coda wave velocity θ and the remnant decorrelation coefficient Kd) will be proportional to the change in crack length within the heterogeneous medium. In this study, the change in crack length through numerical simulation can be simulated by considering the different nonlinear interface areas between the screws and the perforated aluminum plate in the experimental design. Experimental findings demonstrate that the CWI observables are proportional to the nonlinear interface areas, which essentially aligns with previous numerical simulation results. In this paper, suggestions for refining the experimental setup are provided. This guidance is instrumental for further conducting quantitative research on nonlinear interface effects in complex media.

1. Introduction

Coda waves, due to their long and intricate paths, exhibit heightened sensitivity to perturbations in the propagation medium compared to early arriving waves. Initially utilized by seismologists to estimate minor velocity variations while studying the movements of the earth's crust [1–3], the sensitivity of coda waves has since been leveraged for Non-Destructive Testing (NDT) of complex materials and structures [4–6]. The signal processing method known as Coda Wave Interferometry (CWI) monitors subtle changes in a multiple scattering propagation medium by evaluating relative variations in coda wave velocity and waveform [7]. CWI has proven to be highly sensitive to minor disturbances, such as temperature fluctuations [8,9], stress level alterations [4,10], changes in damage state [11,12], and microcrack modifications [13,14]. Zhang et al. [15] recently proposed the Nonlinear Coda Wave Interferometry (NCWI) method, which combines the advantages of CWI with the nonlinear modulation method. This combination is highly sensitive to the physical properties of heterogeneous materials, thus making it widely used for detecting microcracks or early-stage damage [16–19]. The nonlinear effects are accentuated by a strong pump wave in a wide low-frequency band and excited uniformly over the entire inspected material by a high-frequency coda wave, analyzed using the CWI method. NCWI has found utility in assessing the damage level in various materials such as glass [15,20], mortar [21], and concrete [22,23].

Aiming to further elucidate the physical principles and associated parameters of the aforementioned NCWI applications, a series of parametric sensitivity studies of NCWI have been conducted using the Spectral Element Method (SEM). The impact of the strong pump wave is modeled within several Effective Damaged Zones (EDZs), either by altering Young's modulus or by introducing small cracks of varying length, as a response to nonlinear fast dynamic effects [24,25]. Employing the *Stretching* technique, CWI evaluates the correlation coefficient $CC(\theta_k)$ between a perturbed signal and a reference signal with an expansion rate θ_k ($k = 1, 2, \ldots, n$ for different levels of expansion),

* Corresponding author at: School of Electronic and Information Engineering, Changshu Institute of Technology, Changshu 215500, China.
E-mail address: guangzhi.chen@cslg.edu.cn (G. Chen).

https://doi.org/10.1016/j.ndteint.2023.102992
Received 13 July 2023; Received in revised form 26 October 2023; Accepted 5 November 2023
Available online 7 November 2023

which could simulates an global increase/decrease of the propagation velocity in the medium [26]. CWI analysis yields two observable parameters, θ and Kd. θ, which is strongly correlated to velocity changes, is introduced when $CC(\theta_k)$ reaches its maximum value and can be simply denoted as $\theta = \theta_k = \delta v/v$; Kd, the decorrelation coefficient, is introduced as $Kd = 100(1 - CC(\theta))$ and is associated with the degree of distortion caused by changes in the medium. Results indicate that these two CWI parameters are proportional to $S_{EDZ} \times \Delta E$, where S_{EDZ} represents the EDZ surface area and ΔE the change in elastic modulus within the EDZ. Simulations demonstrate that introducing small cracks within the EDZ impacts CWI observables similarly to changes in the elastic modulus. Furthermore, to simulate a more realistic behavior of microcracks, the strong pump wave's influence on the localized microcracked zone is modeled as a small average increase in each crack's length. Consequently, the NCWI method proves valuable for detecting different damaged material states in complex solids, being sensitive to minor changes in a damaged zone's elastic modulus, the emergence of microcracks, or variations in microcrack length.

However, detecting microcracks or closed cracks in highly heterogeneous materials remains a considerable challenge using linear ultrasonic NDT methods. When the excitation is sufficiently strong, Contact Acoustic Nonlinearity (CAN) is activated at the crack level, playing a significant role in nonlinear ultrasonic NDT [27]. CAN pertains to imperfect interfaces, crack opening and closing (clapping), and friction during the application of a strong acoustic excitation, and can be observed through harmonic generation phenomena [28,29]. While CAN has been extensively studied numerically in homogeneous mediums [30–33], it remains challenging or even impossible to create relevant artificial microcracks in solids for CAN experimental studies. Inspired by the experiment conducted by Rivière et al. [34], this paper proposes an experimental protocol to approach this problem approximately. The CAN effects, corresponding to the nonlinear interface behavior, are generated by contacts between a threaded metal plate and a given number of screws. In this way, the nonlinear interface areas are controlled by the screw count, and CAN depends on the screw arrangement on the perforated plate—factors such as the applied torque and the screw threading, for instance. This study considers a perforated aluminum plate, with four configurations examined corresponding to different numbers of screws (N_{screws} = 5, 10, 15) or no screws at all. To mitigate temperature bias on CWI results and enhance experimental repeatability, a same perforated aluminum plate is employed as a reference under identical measurement conditions. The experimental results of NCWI are analyzed with respect to varying numbers of screws in the plates, representing controlled distributed CAN effects, aiming to approximately represent the different nonlinear interface areas in the material [34].

2. Experimental design

2.1. Experimental set-up

In the experiment, two identical aluminum plates are considered, each measuring 30 cm × 30 cm × 2 cm. These plates contain randomly distributed, homogeneous circular voids of ∅ 10 mm each (see Fig. 1). The ratio of the 2D surface area of the circular voids to the total specimen area is approximately 17.6%. Near the top edge of the specimens, 15 of the circular voids are threaded holes, into which varying numbers of screws ($N_{screws} = 0,\ 5,\ 10,\ 15$) can be inserted using a torque wrench controlled at 0.9 N m.

Both plates are positioned vertically and are simply supported by two small pieces of white polyethylene (see Fig. 2). Various piezoelectric transducers employed in this setup are attached to the edges of the plates. Plate (A) is designated as the testing plate, while Plate (B) serves as a reference for controlling thermal bias. On each plate (A and B), two identical transducers function as the source and receiver for the coda measurement.

The probe coda wave is generated and amplified before being transmitted into the specimen, operating within a frequency range of 200 kHz to 800 kHz and lasting 0.2 ms. Simultaneously, the received probe signal, following the probe wave emission, is recorded for a duration of 3 ms using a sampling frequency of 5 MHz and 16-bit amplitude dynamics. The synchronization between excitation and acquisition is facilitated by a 10 MHz reference clock signal. To enhance the signal-to-noise ratio, one recorded coda is set to be an average of 256 successive acquisitions. The repetition frequency is 15 Hz, resulting in an average coda measurement time of less than 1 s. The amplification configuration for the coda measurement remains consistent throughout the experiment. A large-amplitude chirp pump wave, operating at a low frequency range of 15 kHz to 50 kHz, is applied exclusively to plate (A). It is important to highlight that the coda waves used in the testing method comprise multiple scattered waves, which represents a relatively stable state of the propagation medium. As a result, the spatial distribution of the deployed sensors relative to the simulated damaged area, or specifically, the placement of screws, has minimal impact on the experimental results, rendering it negligible. This assertion has been validated in previous numerical simulations and NCWI experiments [20,24]. The entire experiment is conducted in a laboratory under controlled temperature conditions (19 ± 1 °C). Air temperature is monitored by a Rotronic® thermometer positioned between the two specimens.

2.2. Experimental procedure

As depicted in Fig. 3, the entire experimental procedure consists of three sets of monitoring and pump wave application tests. Each test spans approximately 5.19 h, which includes 4.81 h of monitoring and roughly 22.8 min (or 0.38 h) for the strong pump wave application. Throughout the monitoring phase of each test, when the pump waves are not applied, 50 coda signals of 3 ms duration are recorded in both the testing plate (A) and the reference plate (B). The interval between each recording is about 5.7 min. Given the brief duration of each test, the variation in ambient temperature remains minimal.

The pump wave is applied solely to plate (A), yet the number of coda signals recorded is the same for both plates (A and B), using identical measurement parameters. The pump wave application process consists of 20 steps (see Fig. 3). During the initial four steps, A_{pump} remains at 0. It then incrementally increases from 0 dB to 50 dB, with each step increasing by 10 dB. For A_{pump} between 50 dB and 60 dB, the steps progress as follows: 54 dB, 56 dB, and 58 dB. Subsequently, A_{pump} is held at its maximum of 60 dB for the next four steps, after which it is directly decreased to 0 dB, where it remains for the final four steps [15,22]. Each step lasts approximately 68 s, during which four coda signals are continuously recorded.

3. Experimental results

3.1. Dependence of CWI observables on the pump wave amplitude level

3.1.1. CWI results with thermal bias control

The initial set of experimental tests (Exp. Set $N°1$) is conducted under two configurations corresponding to cases with and without 15 screws inserted into both plates (A and B). As outlined in Section 2.2, for each experimental test, a total of 130 signals (that is, 50 monitoring signals and 20 × 4 testing signals with pump wave application) are analyzed using the *Stretching* method. The selected time window ranges from 1.5 ms to 2.0 ms [24]. To ensure that the experimental environment is stable, the 30th recorded signal is chosen as the reference signal for the CWI analysis throughout both the monitoring and pump wave application, which spans roughly 5.19 h. Fig. 4 illustrates the results of one experimental test for two cases, namely, $N_{screws} = 0$ and $N_{screws} = 15$.

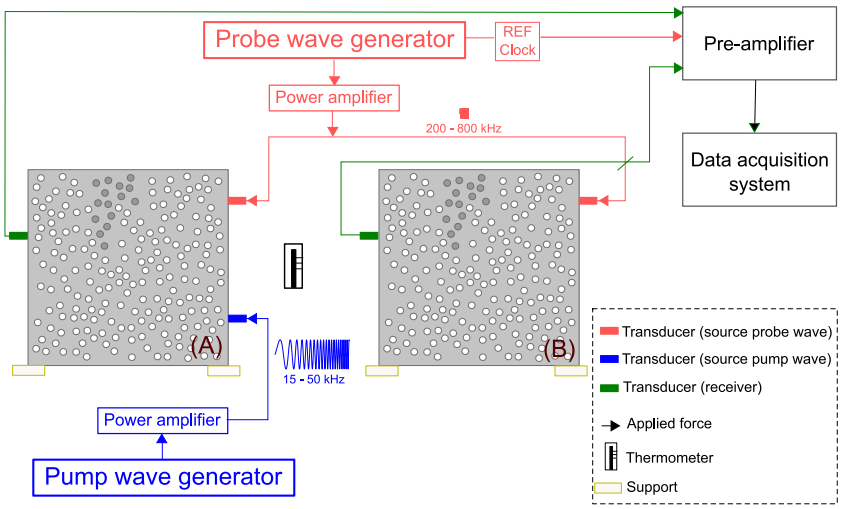

Fig. 1. CWI measurement system with thermal bias control technique.

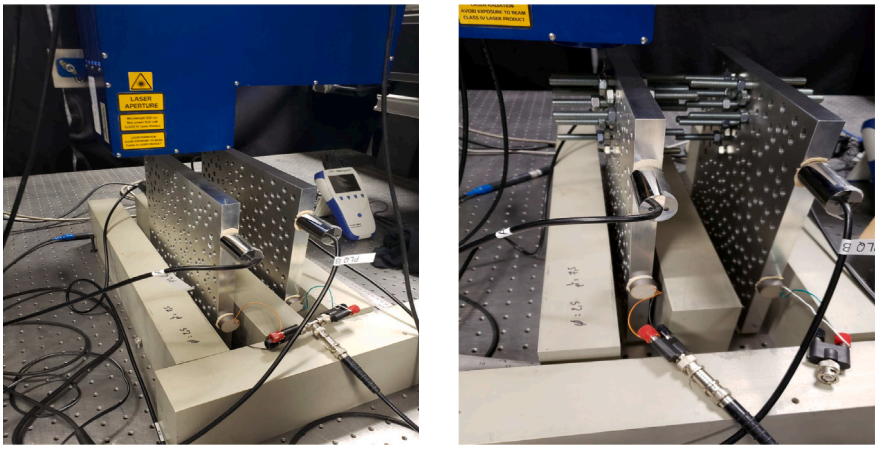

Fig. 2. Photographs of the experimental system: (a) View of the experimental system in the absence of screws in the aluminum plates; (b) Detailed view of the aluminum plates with screws.

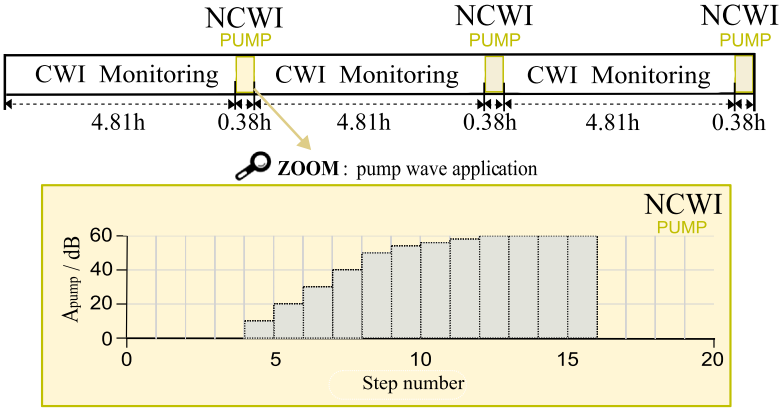

Fig. 3. Schematics of the experimental procedure.

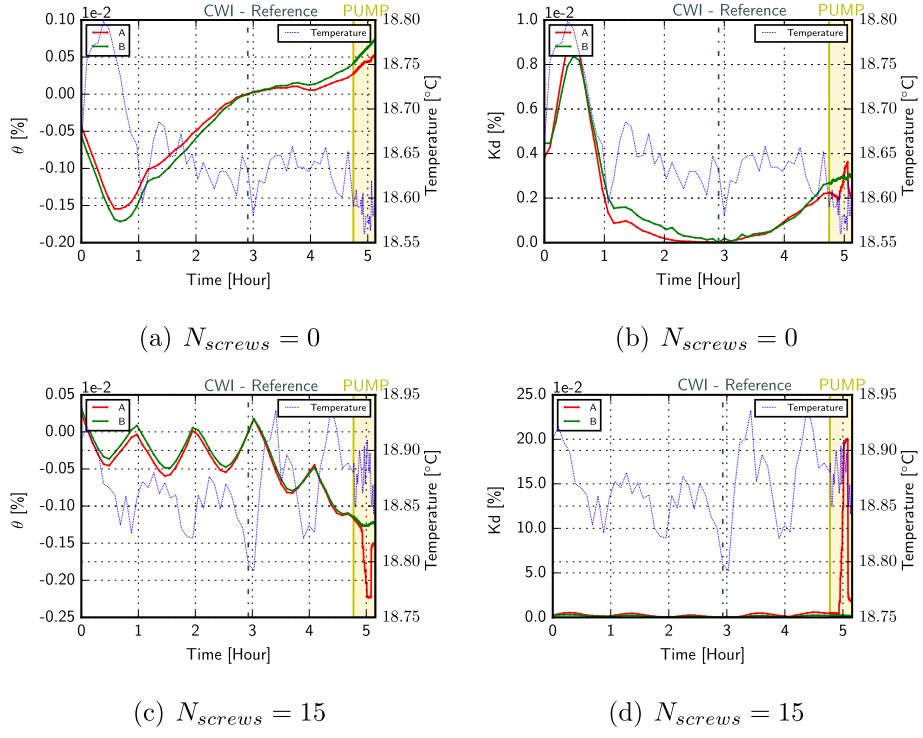

(a) $N_{screws} = 0$ (b) $N_{screws} = 0$

(c) $N_{screws} = 15$ (d) $N_{screws} = 15$

Fig. 4. Exp. Set $N°1$: The dependence of the CWI observables on air temperature for $N_{screws} = 0$ (a)(b) and $N_{screws} = 15$ (c)(d). The temperature fluctuation is represented by a blue dotted line, while the CWI analysis (θ and/or Kd) is depicted by the red line (for the testing specimen A) and the green line (for the reference specimen B). The reference signal in CWI analysis corresponds to the 30th recorded signal, marked with a vertical dotted gray-green line. The pump wave is applied after approximately 4.81 h of monitoring. (a,c) The relative variation in velocity θ versus time; (b,d) The remnant decorrelation coefficient Kd versus time. (For interpretation of the references to color in this figure legend, the reader is referred to the web version of this article.)

The thermally-induced velocity variation of multiple-scattering ultrasonic waves has been observed consistently in various types of materials [8,35,36]. As such, bias control of the environmental temperature is necessary for CWI analysis, given the extreme sensitivity of coda waves to minor velocity variations [4]. Fig. 4 provides real-time temperature fluctuations, illustrated by a red dotted line. The maximum amplitude of temperature variation during the 5-h testing period is 0.25 °C, underscoring the sensitivity of the CWI method to slight temperature variations. In both cases, specimens (A) and (B) exhibit very similar variation trends for the CWI observables (θ and Kd) during the initial pure CWI monitoring period. Fig. 4-a,c reveal that the variation of θ inversely correlates with the temperature variation. For example, a slightly higher temperature (an increase of 0.1 °C) results in a velocity variation in the aluminum plate of −0.0015%. This phenomenon has been similarly observed in other experiments [35,37,38]. While the remnant decorrelation coefficient, Kd, is to a lesser extent influenced by temperature variations, no correction method can be implemented [8,36].

The commencement of the NCWI test for cases $N_{screws} = 0$ (Fig. 4-a,b) and $N_{screws} = 15$ (Fig. 4-c,d) is marked in dark yellow. Clearly, in the case with 15 screws in plate (A), the variations in θ and Kd values are significantly greater than those in the case without screws. In the ensuing NCWI analysis, the first recorded signal during the pump wave application of about 0.38 h (with pump wave amplitude level at the first step of 0 dB) is used as the reference signal. The reference specimen (B) is employed to compensate for the temperature influence during the NCWI test. In the subsequent experimental study, all analyses of the CWI results are temperature-corrected with Eq. (1) [36] for a given time window centered on t_c.

$$\theta(t_c) = \theta_{(A)}(t_c) - \theta_{(B)}(t_c) \tag{1}$$

where $\theta(t_c)$ denotes the temperature-corrected CWI analysis results, abbreviated as θ in the following sections; $\theta_{(A)}(t_c)$ and $\theta_{(B)}(t_c)$ refer to the CWI analysis results corresponding to the test sample Plate (A) and the reference sample Plate (B), respectively.

3.1.2. NCWI results

The NCWI results for both tests (N_{screws} = 0,15) are depicted in Fig. 5-a,b, with the corresponding pump wave amplitude level illustrated in Fig. 5-c. A clear dependence of the NCWI results of the specimen with 15 screws (shown in green) on the pump wave amplitude level A_{pump} is evident: (1) As A_{pump} increases, θ decreases while Kd incrementally increases, especially from $A_{pump} > 50$ dB; (2) When A_{pump} remains at the level of 60 dB, both θ and Kd cease to change and retain their peak values; (3) When decreasing A_{pump} directly back to 0 dB, θ and Kd return to almost their initial values.

Conditioning phenomena of the material are present as θ and Kd do not return directly to their initial values, revealing a slow dynamic effect [20,39–41]. Compared to the NCWI results in the case with 15 screws (in green), the case without screws (in blue) demonstrates no comparable variations throughout the test. However, a minor pump wave amplitude dependence phenomenon is observed in the case without screws, which could be attributed to nonlinear contact activation between the small supporting pieces and the specimen or the overall nonlinearity of the system, inclusive of the measurement chain.

The aluminum plate sample without screws can be construed as a linear propagation medium. Consequently, the reported results on the sample containing screws may reflect the nonlinear contact between the screws and the specimen during the pump wave application. The contacts between the screws and the specimen behave as nonlinear scatterers, and among the potential manifestations of these are (i) an effective material softening phenomenon [15,39,42], (ii) an increased

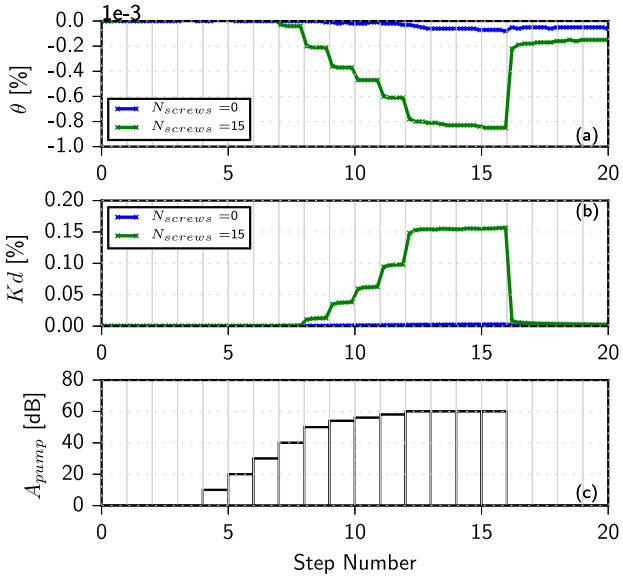

Fig. 5. Exp. Set $N°1$: CWI results versus pump wave amplitude level (A_{pump} in dB) for two distinct cases (N_{screws} = 0,15). (a) The relative variation in velocity θ versus step number; (b) The remnant decorrelation coefficient Kd versus step number; (c) Excitation amplitude of pump waves at each step of the test. (For interpretation of the references to color in this figure legend, the reader is referred to the web version of this article.)

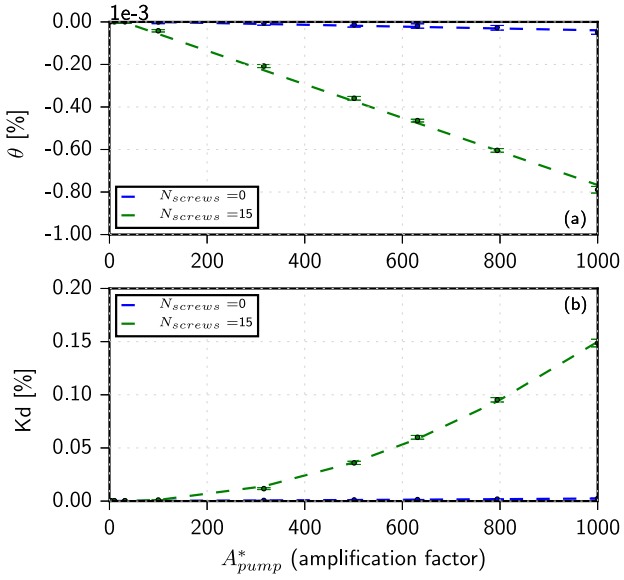

Fig. 6. Exp. Set $N°1$: CWI results versus pump wave amplitude level (linear and normalized A^*_{pump}). (a) The relative variation in velocity θ versus A^*_{pump}; (b) The remnant decorrelation coefficient Kd versus A^*_{pump}. Results in two test conditions are plotted: blue squares for the case with specimens without screws and green pentagrams for the case with screws fixed on. A linear fit for θ versus A^*_{pump} and a quadratic fit for Kd versus A^*_{pump} are provided in corresponding colors. (For interpretation of the references to color in this figure legend, the reader is referred to the web version of this article.)

effective dissipation, (iii) an effective change in the length (or surface) of poorly contacting surfaces (equivalent to the effect of crack length change in the previous study [43]). These experimental results align closely with the studies of cracked specimens in diverse materials, such as glass [15,20], mortar [21], or concrete [22,23].

Fig. 6 plots the results for the first part of the NCWI procedure while increasing the A_{pump} up to 60 dB, with a normalized linear scale pump amplitude level : $A^*_{pump} = A_{pump}/A^{0\ dB}_{pump}$. The error bars account for the standard deviation from three repeated experimental tests for each case (with N_{screws} = 0 or 15). In Fig. 6(a), the value of θ increases with the corresponding increase in A^*_{pump} for the case where N_{screw} = 15. The dashed line shows the best-fit linear regression with fitting quality estimated by coefficient of determination R^2. Since the linear dependence are clearly observed and validated ($R^2 > 0.9$ for all cases), the linear relation connecting θ with A^*_{pump} can be written as: $\theta = \alpha_\theta \cdot A^*_{pump}$, with the slope denoted by α_θ. The results of Kd is plotted in Fig. 6(b) in a same manner, the only difference here being that the dashed line indicates the best-fit of a quadratic regression for the case where N_{screw} = 15. With the fitting quality remaining highly satisfactory, Kd is related to A^*_{pump} with a quadratic relation: $\mathrm{Kd} = \alpha_{\mathrm{Kd}} \cdot A^*_{pump}$, where the quadratic coefficient is denoted by α_{Kd}.

A linear fit for θ versus A^*_{pump} and a quadratic fit for Kd versus A^*_{pump} are found valid, as predicted in [15] for the quadratic hysteretic nonlinearity phenomenon [16,39,44] and in alignment with the numerical studies of previous study where it is posited that elastic and dissipation parameters of the EDZ or the effective crack length change in proportion to the pump amplitude [43]. These relationships have also been observed in other experiments [15,20,21]. Two nonlinear coefficients, denoted as α_θ and α_{Kd}, can be derived, quantifying the global material nonlinearity level. The corresponding values of α_θ and α_{Kd} for different tests are listed in Table 1. These results corroborate that the contacts between the specimen and the screws function as nonlinear scatterers, as similarly observed in [34].

Table 1
Exp. Set $N°1$: Extracted nonlinear coefficients (α_θ and α_{Kd}) from the relationship between CWI observables (θ and Kd) and the linear normalized pump wave amplitude level for specimens without screws ($N_{screws} = 0$) and with 15 screws ($N_{screws} = 15$).

Nonlinear parameters (mean value)	$N_{screws} = 0$	$N_{screws} = 15$
α_θ	-4.349×10^{-8}	-7.893×10^{-7}
α_{Kd}	9.562×10^{-10}	1.548×10^{-7}

3.2. Sensitivity of the NCWI results to the amount of internal solid contact surfaces

Based on previous numerical simulation results [43], it is expected that the CWI observables (θ and Kd) will show a direct relationship with the alteration in crack length in the heterogeneous medium. For a micro-cracked material and considering coda waves in the diffusion regime, the numerical simulation results indicate that the relationships between CWI observables (θ and Kd) and the total change in crack length ΔL^T_{crack} (the product of the relative change in crack length $\Delta L_{crack}/L_{crack}$ and the crack number N_{crack}), which can be formulated as Eqs. (2) and (3).

$$\theta = \alpha_\theta^{\sum L} \times \left(\Delta L^T_{crack}\right) = \alpha_\theta^{\sum L} \times \left(\frac{\Delta L_{crack}}{L_{crack}} \times N_{crack}\right) \quad . \tag{2}$$

$$\mathrm{Kd} = \alpha_{\mathrm{Kd}}^{\sum L} \times \left(\Delta L^T_{crack}\right)^2 = \alpha_{\mathrm{Kd}}^{\sum L} \times \left(\frac{\Delta L_{crack}}{L_{crack}} \times N_{crack}\right)^2 \quad . \tag{3}$$

where $\alpha_\theta^{\sum L}$ and $\alpha_{\mathrm{Kd}}^{\sum L}$ represent the linear and quadratic coefficient, respectively, extracted from the relationship between the CWI observables and the total change in crack length.

To investigate the sensitivity of the NCWI results to the amount of internal solid contact surfaces, a new experimental test (Exp. Set $N°2$) is considered, involving four new configurations corresponding to various numbers of screws on both aluminum plates (the test and reference ones): N_{screw} = 0, 5, 10, 15. Given the stability of the results from the previous study, the same experimental procedure is utilized, albeit with

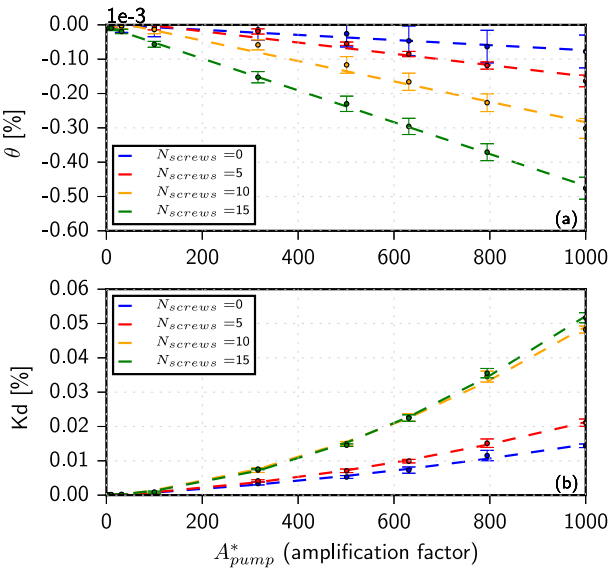

Fig. 7. Exp. Set $N°2$: CWI results versus pump wave amplitude level (linear and normalized A^*_{pump}). (a) The relative variation in velocity θ versus A^*_{pump}; (b) The remnant decorrelation coefficient Kd versus A^*_{pump}. A linear fit for θ versus A^*_{pump} and a quadratic fit for Kd versus A^*_{pump} are provided in the corresponding colors. (For interpretation of the references to color in this figure legend, the reader is referred to the web version of this article.)

a reduced monitoring time and pump wave application time—from 4.81 h to 2.91 h, and 0.38 h to 0.28 h, respectively (Fig. 3).

Fig. 7 illustrates the NCWI results as a function of the normalized linear pump wave amplitude, with error bars accounting for the standard deviation from three repeated experimental tests per case. In Fig. 7(a), from top to bottom, the plot shows θ with increasing A^*_{pump} for progressively increasing damage degrees, with N_{screw} = 0, 5, 10, 15 respectively. Consistent with the previously discussed experimental findings, a linear relationship between θ and A^*_{pump} can be observed in all operational conditions. The corresponding linear coefficient, α_θ, can also be extracted. Similarly, in Fig. 7(b), the results for Kd are plotted using the same approach. For experiments with different number of screws, the quadratic coefficient α_{Kd} can also be obtained. In summary, as the number of screws affixed to the plates increases, the nonlinear effects amplified by the strong pump wave become more pronounced. This enhancement is evidently linked to a larger nonlinear contact surface between the screws and the specimens for larger N_{screws}.

In comparison to the previous tests (Fig. 6), the variations of CWI observables (θ, Kd) are somewhat distinct. The two sets of experimental tests (Exp. Set $N°1$ and $N°2$) were conducted approximately three months apart. The divergence in NCWI results might be attributed to minor physical and chemical modifications to the contact between the steel screws and the aluminum plate, or the wearing of the threads relative to the initial experiments. Achieving full control of the internal contacting surface is difficult, given that nonlinear acoustic phenomena in these cases are driven by nanoscale and microscale phenomena.

The nonlinear coefficient α_θ varies linearly with N_{screws} (Fig. 8-a) as anticipated, based on the previous numerical results (Eq. (2)). However, a linear dependence between α_{Kd} and N_{screws} appears more pertinent than a quadratic one in the experimental tests (Fig. 8-b), conflicting with the numerical results that predict a quadratic dependence (Eq. (3)). Fig. 7-b reveals that the Kd values for N_{screws} = 10 and N_{screws} = 15 are remarkably similar, an unexpected finding. The Kd results in this experiment are relatively unreliable compared to θ results, which could be related to the experimental setup:

1. The specimen is situated on two small white polyethylene pieces on its bottom side, the strong pump wave may have activated the nonlinear contact between the specimen and these supports. The contact between the specimen and the supports is challenging to precisely control for each different experimental test when affixing or removing the screws.
2. Even though a controlled torque wrench of 0.9 N m was used during the screwing process, the method of attaching the screws to the specimen could not be controlled precisely in the same manner with the same force. The process of inserting screws into a metal plate has a complex effect on the internal stress field within the material. Moreover, the variability associated with each screwing process can alter both the total and effective nonlinear contact surface between the specified number of screws and the specimen. These factors can potentially influence the NCWI results.
3. Previous numerical studies were conducted considering a 2D model, but the actual geometry of the aluminum plate in the experiment is in 3D with a plate thickness of 20 mm. Furthermore, the screws are inserted into the plate to protrude from both sides, undoubtedly affecting the NCWI results.
4. To ensure stability in the NCWI results, the interval between different experimental tests was relatively long (>24 h). Although the laboratory temperature was controlled (19 ± 1 °C), minor modifications linked to contact pressures, creep, or chemical reactions in contact with the steel screws and the aluminum plates may occur.
5. Applying a strong pump wave to the specimen could lead to irreversible microstructural modifications, especially in instances where the screws are affixed to the plates. These micro-modifications would likely influence the values of Kd, which evaluate waveform distortions.

The above hypotheses align with another set of experiments, not presented here, in which the strength of screw threads was not controlled.

4. Conclusion

The global assessment of complex material damage levels utilizing the NCWI method is addressed through experimental studies in this paper. An experimental protocol is put forward, facilitating a quantitative study of nonlinear interface effects. This is accomplished experimentally by introducing screw contact in a perforated plate. Two identical perforated aluminum plates, with a surface ratio of circular voids equating to 17.6%, are employed in this study. The voids are randomly spaced in the plate, with 15 potential placements for steel screws. One of the plates serves as a reference for controlling experimental temperature bias. The nonlinear contacts between the screws and the specimen are accentuated by a strong pump wave across a wide broad range of low frequencies. These effects are observed by comparing the coda waves for varying pump wave levels. Four cases, ranging from zero to fifteen screws affixed to the specimen, are evaluated. As anticipated, a linear (respectively, quadratic) relationship between θ (respectively, Kd) and the pump wave amplitude A_{pump} is obtained. With an increasing number of screws N_{screws}, the nonlinear coefficient α_θ (extracted from the θ versus A_{pump} relation) is found to demonstrate a linear relationship with N_{screws}. However, deviating from the numerical results (Eq. (3)), instead of a quadratic relationship between α_{Kd} (Kd versus A_{pump}), a linear one emerges. Additionally, for the cases of 10 and 15 screws, the Kd values remain remarkably close, indicating that the evaluations of waveform distortions are less reliable than those of velocity variations. This variability could be attributed to multiple experimental control details that could potentially be enhanced in future studies. Despite these potential limitations, the experimental results demonstrate that the nonlinear contact between the aluminum plates and the threaded screws can effectively approximate the CAN effects and provide a representation of distributed nonlinear interfaces in the material. This enables a quantitative study of such damage in complex materials, paving the way for further exploration in this field.

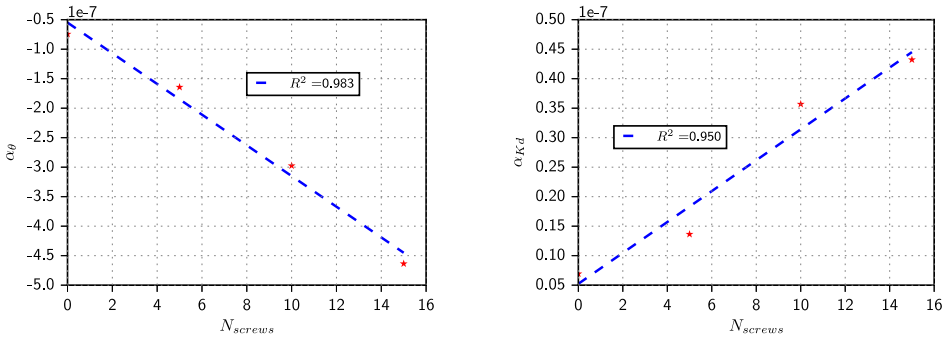

Fig. 8. Exp. Set $N°2$: Nonlinear coefficients. (a) α_θ versus N_{screws} and (b) α_{Kd} versus N_{screws}.

CRediT authorship contribution statement

Guangzhi Chen: Conceptualization, Data curation, Formal analysis, Investigation, Methodology, Software, Visualization, Writing – original draft, Writing – review & editing. **Odile Abraham:** Conceptualization, Funding acquisition, Project administration, Resources, Supervision, Validation, Writing – review & editing. **Damien Pageot:** Formal analysis, Methodology, Software, Visualization. **Olivier Durand:** Formal analysis, Investigation, Resources, Visualization. **Mathieu Chekroun:** Conceptualization, Supervision, Validation, Writing – review & editing. **Vincent Tournat:** Conceptualization, Funding acquisition, Project administration, Supervision, Validation, Writing – review & editing.

Declaration of competing interest

The authors declare that they have no known competing financial interests or personal relationships that could have appeared to influence the work reported in this paper.

Data availability

The data that has been used is confidential.

Acknowledgments

This research was supported by the RFI LMAc (Recherche Formation Innovation Le Mans Acoustique), founded by the Région Pays-de-la-Loire (France).

References

[1] Aki K, Chouet B. Origin of coda waves : Source, attenuation, and scattering effects. J Geophys Res 1975;80(23):3322–42.
[2] Poupinet G, Ellsworth WL, Fréchet J. Monitoring velocity variations in the crust using earthquake doublets : an application to the Calaveras fault, California. J Geophys Res 1984;89:5719–31.
[3] Grêt A, Snieder R, Ozbay U. Monitoring in situ stress changes in a mining environment with coda wave interferometry. Geophys J Int 2006;167(2):504–8.
[4] Larose E, Hall S. Monitoring stress related velocity variation in concrete with a 2×10^{-5} relative resolution using diffuse ultrasound. J Acoust Soc Am 2009;125(4):1853–6.
[5] Planès T, Larose E. A review of ultrasonic Coda Wave Interferometry in concrete. Cem Concr Res 2013;53:248–55.
[6] Niederleithinger E, Wolf J, Mielentz F, Wiggenhauser H. Embedded ultrasonic transducers for active and passive concrete monitoring. Sensors 2015;15:9756–72.
[7] Snieder R. The theory of coda wave interferometry. Pure Appl Geophys 2006;163:455–73.
[8] Weaver RL, Lobkis OI. Temperature dependence of diffuse field phase. Ultrasonics 2000;38(1–8):491–4.
[9] Zhang Y, Abraham O, Larose E, Planes T, Duff AL, Lascoup B, Tournat V, Guerjouma RE, Cottineau L-M, Durand O. Following stress level modification of real seize concrete structure with coda wave interferometry (CWI). AIP Conf Proc 2011;1335(1):1291–8.
[10] Renaud G, Rivière J, Haupert S, Laugier P. Anisotropy of dynamic acoustoelasticity in limestone, influence of conditioning, and comparison with nonlinear resonance spectroscopy. J Acoust Soc Am 2013;133(6):3706–18.
[11] Schurr DP, Kim J-Y, Sabra KG, Jacobs LJ. Damage detection in concrete using coda wave interferometry. NDT & E Int 2011;44(8):728–35.
[12] Niederleithinger E, Wang X, Herbrand M, Mueller M. Processing ultrasonic data by coda wave interferometry to monitor load tests of concrete beams. Sensors 2018;18(1971).
[13] Becker J, Jacobs LJ, Qu J. Characterization of cement-based materials using diffuse ultrasound. J Eng Mech 2003;129(12):1478–84.
[14] Quiviger A, Payan C, Chaix JF, Garnier V, Salin J. Effect of the presence and size of a real macro-crack on diffuse ultrasound in concrete. NDT & E Int 2012;45(1):128–32.
[15] Zhang Y, Tournat V, Abraham O, Durand O, Letourneur S, Duff AL, Lascoup B. Nonlinear mixing of ultrasonic coda waves with lower frequency-swept pump waves for a global detection of defects in multiple scattering media. J Appl Phys 2013;113(6):064905.
[16] Guyer RA, Johnson PA. Nonlinear mesoscopic elasticity: Evidence for a new class of materials. Phys Today 1999;52(4):30–6.
[17] Ten Cate JA. Slow dynamics of earth materials: An experimental overview. Pure Appl Geophys 2011;168(12):2211–9.
[18] Blanloeuil P, Rose LRF, Guinto JA, Veidt M, Wang CH. Closed crack imaging using time reversal method based on fundamental and second harmonic scattering. Wave Motion 2016;66:156–76.
[19] Smagin N, Trifonov A, BouMatar O, Aleshin V. Local damage detection by nonlinear coda wave interferometry combined with time reversal. Ultrasonics 2020;108:106226.
[20] Zhang Y, Tournat V, Abraham O, Durand O, Letourneur S, Duff AL, Lascoup B. Nonlinear coda wave interferometry for the global evaluation of damage levels in complex solids. Ultrasonics 2017;73:245–52.
[21] Hilloulin B, Zhang Y, Abraham O, Loukili A, Grondin F, Durand O, Tournat V. Small crack detection in cementitious materials using nonlinear coda wave modulation. NDT & E Int 2014;68:98–104.
[22] Legland J-B, Zhang Y, Abraham O, Durand O, Tournat V. Evaluation of crack status in a meter-size concrete structure using the ultrasonic nonlinear coda wave interferometry. J Acoust Soc Am 2017;142(4):2233–41.
[23] Qu S, Hilloulin B, Saliba J, Sbartaï M, Abraham O, Tournat V. Imaging concrete cracks using Nonlinear Coda Wave Interferometry (INCWI). Constr Build Mater 2023;391:131772.
[24] Chen G, Pageot D, Legland. J-B, Abraham. O, Chekroun. M, Tournat V. Numerical modeling of ultrasonic coda wave interferometry in a multiple scattering medium with a localized nonlinear defect. Wave Motion 2017;(72):228–43.
[25] Chen G, Pageot D, Abraham O, Zhang Y, Chekroun M, Tournat V. Nonlinear Coda Wave Interferometry: Sensitivity to wave-induced material property changes analyzed via numerical simulations in 2D. Ultrasonics 2019;99:105968.
[26] Snieder R, Grêt A, Douma H, Scales J. Coda wave interferometry for estimating nonlinear behavior in seismic velocity. Science 2002;295(5563):2253–5.
[27] Solodov LY, Krohn N, Busse G. CAN : an example of nonclassical acoustic nonlinearity in solids. Ultrasonics 2002;40:621–5.
[28] Burnham NA, Kulik AJ, Gremaud G, Gallo PJ, Oulevey F. Scanning local-acceleration microscopy. J Vac Sci Technol B 1996;14(2):794–9.
[29] Korshak BA, Solodov IY, Ballad EM. {Dc} effects, sub-harmonics, stochasticity and memory for contact acoustic non-linearity. Ultrasonics 2002;40(18):707–13.
[30] Hirose S, Achenbach J. Higher harmonics in the far field due to dynamic crack-face contacting. J Acoust Soc Am 1993;93(1):142–7.

[31] Pecorari C. Nonlinear interaction of plane ultrasonic waves with an interface between rough surfaces in contact. J Acoust Soc Am 2003;113(6):3065–72.
[32] Blanloeuil P, Meziane A, Bacon C. 2D finite element modeling of the non-collinear mixing method for detection and characterization of closed cracks. NDT & E Int 2015;76:43–51.
[33] Delrue S, Aleshin V, Truyaert K, Bou Matar O, Van Den Abeele K. Two dimensional modeling of elastic wave propagation in solids containing cracks with rough surfaces and friction - Part II: Numerical implementation. Ultrasonics 2018;82:19–30.
[34] Rivière J, Renaud G, Haupert S, Talmant M, Laugier P, Johnson PA. Nonlinear acoustic resonances to probe a threaded interface. J Appl Phys 2010;107:124901.
[35] Lu Y, Michaels JE. A methodology for structural health monitoring with diffuse ultrasonic waves in the presence of temperature variations. Ultrosonics 2005;43:717–31.
[36] Zhang Y, Abraham O, Tournat V, Duff AL, Lascoup B, Loukili A, Grondin F, Durand O. Validation of a thermal bias control technique for Coda Wave Interferometry (CWI). Ultrasonics 2013;53(3):658–64.
[37] Asay JR, Chhabildas LC. Determination of the shear strength of shock compressed 6061-T6 aluminum. In: Shock waves and shock-strain-rate phenomena in metals. 1981.
[38] Dodson JC, Inman DJ. Investigating the thermally induced acoustoelastic effect in isotropic media with Lamb waves. J Acoust Soc Am 2014;136(5).
[39] Johnson PA, Sutin A. Slow dynamics and anomalous nonlinear fast dynamics in diverse solids. J Acoust Soc Am 2005;117:124.
[40] Vu QA, Garnier V, Chaix JF, Payan C, Lott M, Eiras JN. Concrete cover characterisation using dynamic acousto-elastic testing and Rayleigh waves. Constr Build Mater 2016;114:87–97.
[41] Eiras JN, Vu QA, Lott M, Payá J, Garnier V, Payan C. Dynamic acousto-elastic test using continuous probe wave and transient vibration to investigate material nonlinearity. Ultrasonics 2016;69:29–37.
[42] Larose E, Obermann A, Digulescu A, Planes T, Chaix JF, Mazerolle F, Moreau G. Locating and characterizing a crack in concrete with diffuse ultrasound: A four-point bending test. J Acoust Soc Am 2015;138(1):232–41.
[43] Chen G, Zhang Y, Abraham O, Pageot D, Chekroun M, Tournat V. Numerical parametric study of Nonlinear Coda Wave Interferometry sensitivity to microcrack size in a multiple scattering medium. Ultrasonics 2021;4:116.
[44] Guyer RA, Johnson PA. Nonlinear mesoscopic elasticity. Wiley-VCH; 2009.